CREEP RESISTANCE OF SINGLE CRYSTAL SUPERALLOYS CMSX-4 AND CM186LC

PETR LUKÁŠ*, †JOSEF ČADEK, LUDVÍK KUNZ, MILAN SVOBODA, JAN KLUSÁK

Institute of Physics of Materials, Academy of Sciences of the Czech Republic, Žižkova 22, 616 62 Brno, Czech Republic

Received 20 October 2004, accepted 16 November 2004

The high resistance of single crystals of nickel-base superalloys to plastic deformation and their superior strength properties at high temperatures are mainly due to the reinforcing γ' precipitates. The paper deals with the properties and structures of two superalloys differing in the γ/γ' morphology. The creep resistance of the $\langle 001 \rangle$, $\langle 011 \rangle$ and $\langle 111 \rangle$ oriented single crystals of superalloys CMSX-4 and CM186LC was compared on the basis of creep rupture curves, creep deformation curves and accompanying development of microstructures in the temperature interval 750 to 950 °C. Further, the effect of notches on creep behaviour and the origin of creep cracks were examined.

K e y w o r d s: creep, single crystal nickel base superalloys, γ/γ' distribution, notch effect

1. Introduction

Nickel base superalloys in single crystal form are widely used for high temperature applications because of their good resistance to plastic deformation. More specifically, it can be stated that the use of single-crystal components in aero--engine gas turbines is now well established. Since beginning of the early seventies several million parts have been produced so far. Considering actual situation, single-crystal components are no longer confined to military engines, where they were first tested, but have entered service in the turbines of civil engines [1]. There are two factors making single-crystal superalloys superior to conventionally cast superalloys. First, the absence of grain boundary strengthening elements allows heat treatments at higher temperatures. This permits the γ' microstructure to be refined and thereby increases the creep strength of the alloy. The second reason is that the $\langle 001 \rangle$ oriented single crystals – which are used for practical applications

*corresponding author, e-mail: lukas@ipm.cz

– are characterized by a low Young's modulus, and therefore their thermal fatigue behaviour is considerably improved by minimizing the thermal stresses [2].

To the currently most widely used single-crystal aircraft turbine blade superalloys belongs alloy CMSX-4. The CMSX-4 is a second generation single crystal superalloy containing 3 % Re. Rhenium partitions mainly to the γ matrix, retards coarsening of the γ' strengthening phase, and increases the γ/γ' misfit. The alloy is capable of full γ' solutioning. The alloy disadvantage is that the solution heat treatment stage is expensive. Single crystals of alloy CM186LC, which do not need the expensive solution heat treatment, are seen as a potential low cost alternative for industrial power generating gas turbines; a complex multi-phase microstructure is the disadvantage of this superalloy.

The gas turbine inlet temperature in industrial turbines often exceeds 1300 ℃, leading to a blade metal temperature of between 750 to 950 ℃. Comparison of creep life-time data in the temperature interval 750 to 950 ℃ for single crystals of CM186LC with those for single-crystalline CMSX-4 showed that the CM186LC exhibited shorter creep lives [3]. In our preceding paper [4] we have shown for the temperature of 850 ℃ and crystal axis orientation $\langle 001 \rangle$ that the creep rate of CM186LC was higher than that of CMSX-4 for the whole lifetime. The aim of the present paper is to compare creep resistance of the $\langle 001 \rangle$, $\langle 011 \rangle$ and $\langle 111 \rangle$ oriented single crystals of superalloys CM186LC and CMSX-4 on the basis of creep rupture curves, creep deformation curves and accompanying development of microstructures in the temperature interval 750 to 950 ℃. Moreover, for the temperature of 850 ℃ also the effect of notches on creep resistance will be presented.

2. Material and experimental procedures

Single crystals of both superalloys were kindly provided by Howmet Ltd., England in the framework of the COST 501 Round III programme (CMSX-4) and in the framework of a COST 522 programme (CM186LC). The nominal chemical composition of the alloys is given in Table 1. It can be seen that the main difference in the chemical compositions of CM186LC and CMSX-4 lies in the content of carbide-forming elements, such as carbon, hafnium and boron. Both the superalloys consist of γ matrix and reinforcing γ' precipitates.

Table 1. Nominal chemical composition of superalloys CMSX-4 and CM186LC (wt.%)

	Ni	Co	Cr	Mo	Al	Ti	Ta	W
CMSX-4	60	9.7	6.5	0.6	5.6	1.04	6.5	6.4
CM186LC	60	9.3	6.1	0.51	5.7	0.73	3.4	8.4
	Re	Nb	B	Hf	Zr	Fe	C	
CMSX-4	2.9	<0.05	0.002	0.11	0.001	0.038	0.0025	
CM186LC	2.9	–	0.016	1.4	0.004	0.027	0.062	

The lattice misfit between the γ and γ' phases is negative. The main difference in the structure of CM186LC and CMSX-4 is the degree of regularity of the γ/γ' phase distribution [3, 5]. The as-cast microstructure of single crystal CM186LC consists of eutectic γ/γ' islands (in the interdendritic regions) surrounded by the primary γ phase with a finely precipitated γ' phase (within the dendrites). There are no eutectic islands in the fully heat-treated single crystal of CMSX-4. The shape of the γ' particles within the eutectic colonies is highly irregular and that their size varies between 0.2 and 10 μm. Shape of the γ' particles in the dendritic regions is cuboidal and their size varies in a small interval, between 0.3 and 0.4 μm. One example of the γ/γ' phase distribution in CM186LC is shown in Fig. 1a. The shape and size of the γ' precipitates in the eutectic colony are seen to be highly irregular; outside the eutectic region (upper right-hand and upper left-hand parts of the micrograph) the γ' precipitates are cuboidal with the size about 0.4 μm. The total volume fraction of the γ' phase is 70 to 80 %; the volume fraction of the eutectic colonies is between 20–25 %. Contrary to the case of CM186LC, the γ/γ' arrangement in the CMSX-4 is quite regular within the whole volume of the crystal (Fig. 1b). The mean size of the γ' particles is about 0.5 μm and their volume fraction is about 70 % [6]. Both the alloys contain casting pores and CM186LC contains also primary carbides predominantly precipitated in eutectic colonies.

The testing was carried out on specimens with the nominal single crystal axis orientation either $\langle 001 \rangle$ or $\langle 011 \rangle$ or $\langle 111 \rangle$. The crystallographic orientation of the specimens did not deviate more than 8 degrees from the ideal direction. Two

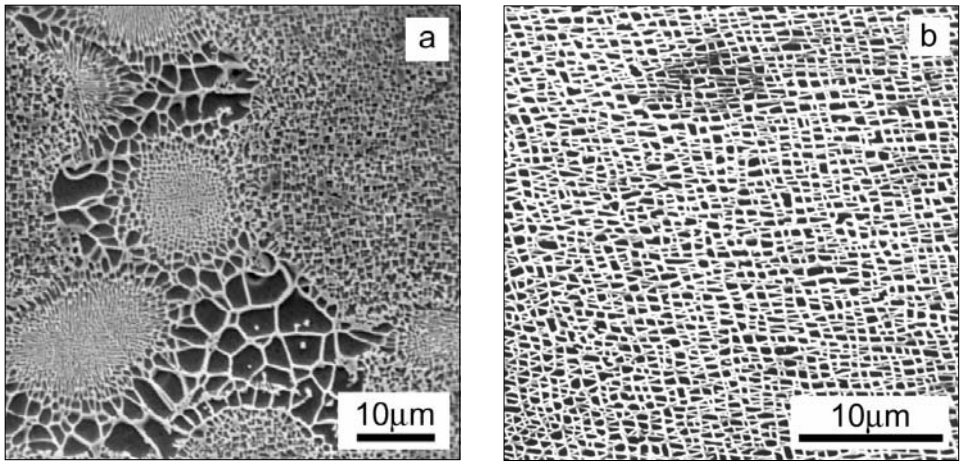

Fig. 1. SEM micrographs of γ/γ' distribution. (a) CM186LC, (b) CMSX-4.

types of specimens were machined from the as-cast bars: (i) smooth specimens with the gauge diameter of 3 mm and the gauge length of 50 mm and (ii) notched specimens with the 5 mm gauge diameter having in the middle of the gauge length a semicircular circumferential notch with the radius of 1 mm. The theoretical (elastic) stress concentration factor for this geometry is $K_t = 1.66$ [7]. The final operation of the machining was a fine grinding. The creep tests were performed in creep machines equipped with data acquisition system at 750, 850 and 950 °C in air under both constant-load and partly also under constant-stress conditions. For CMSX-4 crystals of the orientation ⟨001⟩ several creep tests were carried out also at 800 and 1000 °C. Thin foils for TEM analysis were obtained by mechanical polishing and twin-jet thinning from the failed specimens. Fracture surfaces were examined by means of SEM.

3. Results and discussion

3.1 Creep life

Creep life, i.e. the time to total separation of specimen, depends both on the orientation and on the temperature. Fig. 2 shows examples of the creep rupture curves, i.e. the dependences between the applied stress and the time to rupture. The curves in Fig. 2a were obtained on specimens of ⟨011⟩ orientation and the curves in Fig. 2b on specimens of ⟨111⟩ orientation at a temperature of 850 °C. For the same applied stress the time to rupture is longer for CMSX-4. The creep tests presented in this paper for all temperatures and orientations cover time range from several tens to several thousands hours. Within this range the alloy CM186LC

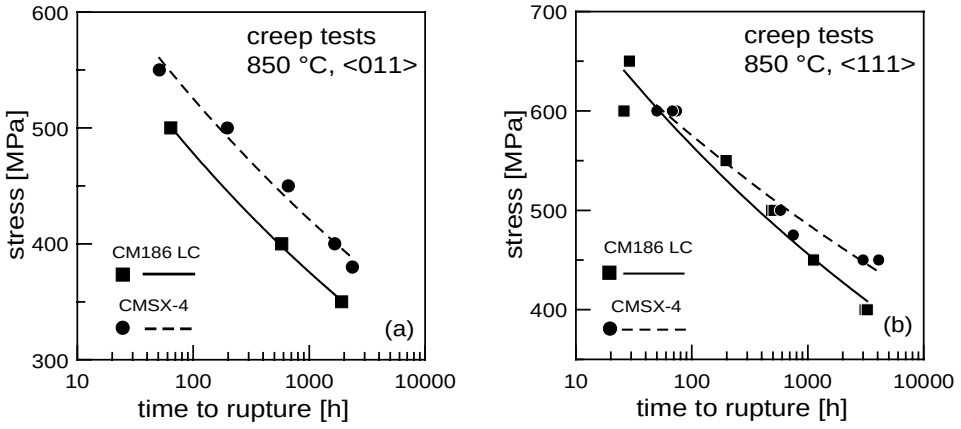

Fig. 2. Creep rupture curves at a temperature of 850 °C. (a) orientation ⟨011⟩, (b) orientation ⟨111⟩.

always exhibits shorter creep life than the alloy CMSX-4 for the same applied stress. This holds also for all test temperatures and orientations. For the practical applications the region of longer lives is of particular importance. Therefore the following quantitative comparison of the two tested superalloys will be carried out on the basis of creep strength at 1000 hours, denoted as σ_{1000}. The values of this creep strength were obtained by means of interpolation from the rupture curves of the type presented in Figs. 2a and 2b. Fig. 3 shows the temperature dependence of σ_{1000} for the orientation $\langle 001 \rangle$. It can be seen that the CMSX-4 is superior to the CM186LC. This superiority expressed in terms of temperature is about 35 ℃ and in terms of stress it is about 80 MPa. Fig. 4 displays the creep strength at 1000 hours for the three tested orientations and for two test temperatures. The recorded data clearly prove that the CMSX-4 superiority, as the values of σ_{1000} for CMSX-4 are always higher than those for CM186LC. Quantitatively, the differences between the values of σ_{1000} for CMSX-4 and for CM186LC are: (i) 80 MPa for orientation $\langle 001 \rangle$ and both temperatures, (ii) 50 MPa for orientation $\langle 011 \rangle$ and both temperatures and (iii) 40 MPa for orientation $\langle 111 \rangle$ and temperature 850 ℃, and 100 MPa for orientation $\langle 111 \rangle$ and temperature 950 ℃. Another interesting point is the ranking of orientations from the point of view of creep resistance. The value of σ_{1000} can be taken as a measure of the alloy creep resistance in such a way that the higher the σ_{1000}, the higher the creep resistance. From that point of view the orientation $\langle 111 \rangle$ is comparable to the orientation $\langle 001 \rangle$ at 850 ℃, but clearly superior to the orientation $\langle 001 \rangle$ at 950 ℃. This holds for both the superalloys. Turbine blades are

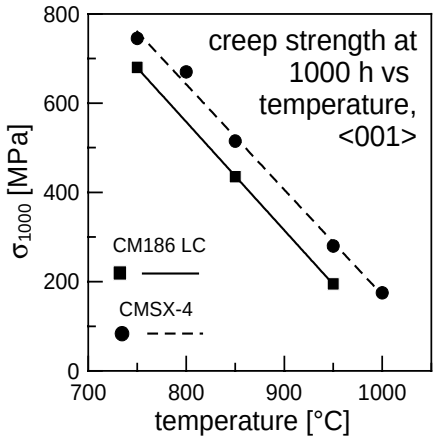

Fig. 3. Temperature dependence of creep strength at 1000 hours.

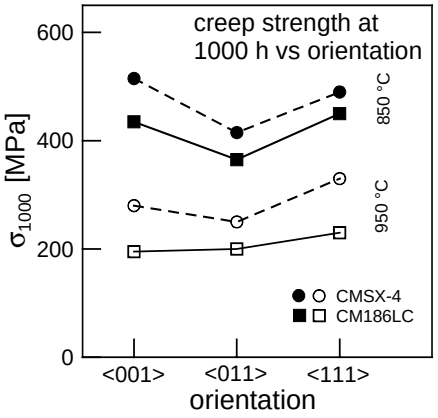

Fig. 4. Creep strength at 1000 hours for the three tested orientations and for two test temperatures.

primarily cast with the ⟨001⟩ orientation along the blade axis. The results presented in Fig. 4 indicate that if the creep resistance were taken as the only criterion, the more suitable orientation would be ⟨111⟩. Other criteria like resistance against low cycle fatigue and ease of casting support the blade orientation ⟨001⟩.

3.2 Creep deformation curves

The common feature of all the creep deformation curves determined on the studied superalloys of all three orientations under all test temperatures is the absence of secondary creep stage characterized by a constant creep rate. This can be best seen in the differentiated form of the creep deformation curves, i.e. in plots creep rate vs. creep strain, which are shown in Figs. 5 and 6. For a temperature of 950 °C the primary creep stage (fall of creep rate with increasing creep strain) is replaced after relatively small creep strain by the tertiary creep stage (increase of creep rate with increasing creep strain); there is no period of constant creep rate and the minimum creep rates thus correspond to the inflexion points on the curves shown in Fig. 5. Creep deformation curves at 850 °C (not shown here) have the same shape as the just presented curves at 950 °C. In contrast to tests at 950 °C and 850 °C, the tests at a temperature of 750 °C show a sigmoidal shape of the differentiated creep deformations curves. This behaviour is most expressive for the orientation ⟨001⟩. In Fig. 6 it can be seen that the minimum creep rates (inflexion points on the curves) correspond to very large creep strains, which in

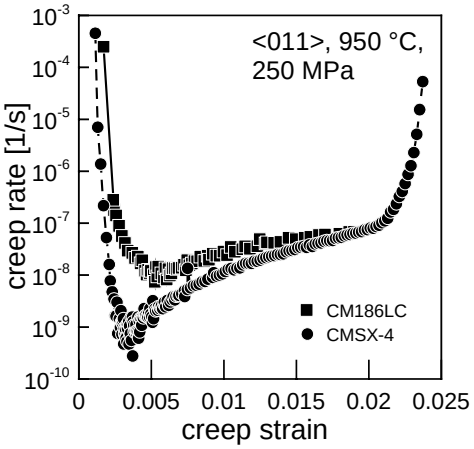

Fig. 5. Differentiated creep deformation curves for temperature 950 °C, orientation ⟨011⟩ and applied stress 250 MPa.

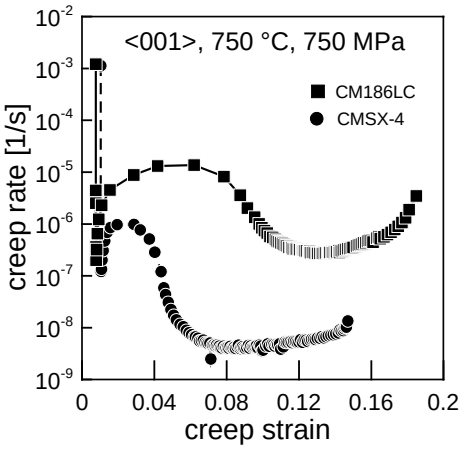

Fig. 6. Differentiated creep deformation curves for temperature 750 °C, orientation ⟨001⟩ and applied stress 750 MPa.

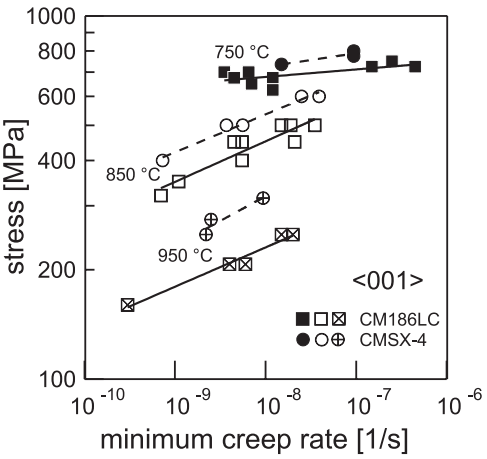

Fig. 7. Stress dependence of minimum creep rate for orientation ⟨001⟩.

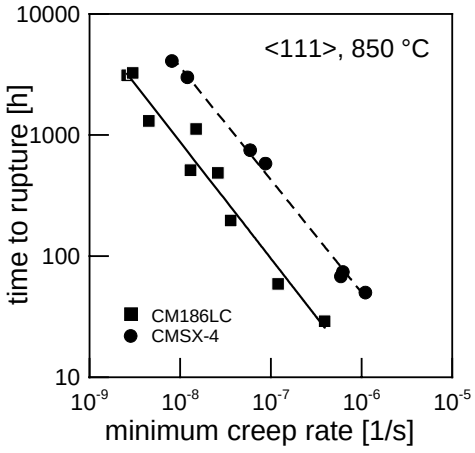

Fig. 8. Monkman-Grant's diagram for orientation ⟨111⟩ and temperature 850 °C.

turn correspond to very substantial fractions of the total creep life. Each pair of curves shown in Figs. 5 and 6 for the two tested superalloys corresponds to the same applied stress. Thus it is possible to compare directly the resistance of the superalloys against creep deformation: the creep rate of CM186LC is higher than that of CMSX-4 for the whole lifetime, in other words, the deformation process in CM186LC is "faster" than that in CMSX-4. The last statement is valid generally for all the applied stresses.

The values of the minimum creep rate determined as the inflexion points on the differentiated creep deformation curves depend on the applied stress and temperature. This is shown for the orientation ⟨001⟩ in Fig. 7. There are three remarkable points of the presented result: (i) the relations between stress and minimum creep rate can be well approximated by power law dependences, (ii) for the same values of the minimum creep rate the stress increases with decreasing temperature and (iii) for the same values of the minimum creep rate the stress corresponding to CMSX-4 is higher than that for CM186LC.

Monkman-Grant's diagram relates the creep rupture data with the creep deformation data, specifically the time to failure with the minimum creep rate. One example of this dependence is presented in Fig. 8. It can be seen that the experimental points can be approximated by straight lines in this log-log plot, which means that there is power law relation between the two quantities. For the same orientation and temperature the line for CMSX-4 lies above the line for CM186LC. The shift between the two lines is relatively large in the presented case. In some

other cases (especially for the orientation ⟨001⟩) the shift is almost negligible and the experimental points for both superalloys can be covered by one scatter band.

3.3 Structural changes

There are two types of structural changes that resulted from creep process: (i) changes in γ/γ' morphology and (ii) changes in dislocation arrangement.

As the tested superalloys are negative misfit alloys, formation of rafts consisting of the γ' phase in the form of plates perpendicular to the stress axis can be expected [e.g. 8 and 9]. This has been observed only in specimens crept at 950 ℃; at lower temperatures the γ/γ' morphology remained untouched by creep deformation. One example of the rafted morphology is shown in Fig. 9. Such rafted structure was formed in dendritic region from regular γ' pattern in a CM186LC specimen crept at 950 ℃. It can be seen that the γ' particles form irregular and often imperfect rafts roughly perpendicular to the stress axis. Exactly the same appearance of the γ/γ' morphology was observed in the whole volume of the CMSX-4 specimens crept at 950 ℃. On the other hand, there is no clear evidence that the γ/γ' structure in the eutectic islands of CM186LC specimens underwent changes during creep deformation. Figure 10 shows the γ/γ' morphology in and near to an eutectic island of a CM186LC specimen crept at 950 ℃. It can be seen that the very large γ' particles typical for the eutectic islands exhibit no tendency to directional

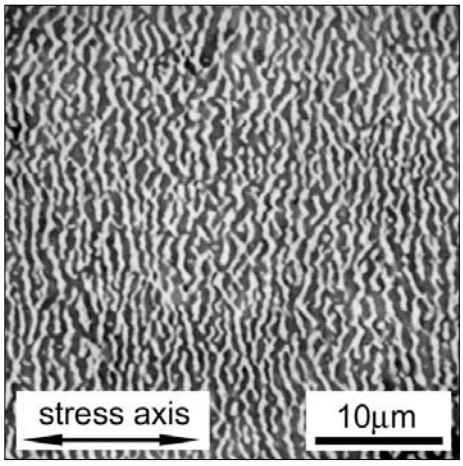

Fig. 9. Rafted γ/γ' structure in dendritic region of a CM186LC specimen crept at 950 ℃. SEM micrograph.

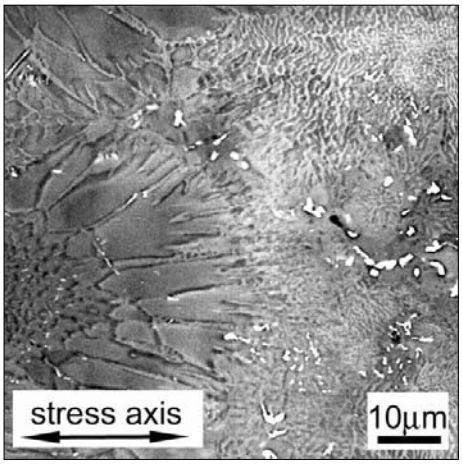

Fig. 10. γ/γ' structure in and near to an eutectic island of a CM186LC specimen crept at 950 ℃. SEM micrograph.

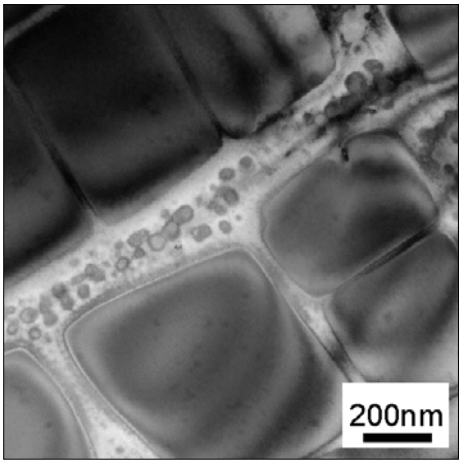

Fig. 11. TEM micrograph of a virgin specimen of CM186LC alloy (dendritic region).

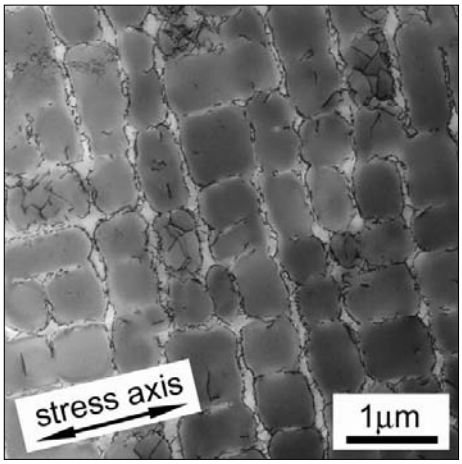

Fig. 12. Dislocation structure in a CMSX-4 specimen after creep exposure at 850 °C.

coarsening. Such large γ' particles have been observed also in the virgin material. Only in the upper right hand corner – far from the eutectic island – a clear rafting is present. Fig. 10 also shows that there is a high number of carbides and casting pores (white spots) in the eutectic regions.

Transmission electron microscopy examination of virgin specimens proved that the crystals are largely free of dislocations. This is shown in Fig. 11 for a CM186LC specimen (dendritic region). Both the γ' cubes and the γ channels can be seen, but there are no dislocations. In some of the γ channels in CM186LC alloy small spherical γ' particles (diameter 20 to 50 nm) were found; no such particles could be found in CMSX-4 crystals. Dislocation structure after creep exposure of a CMSX-4 specimen is shown in Fig. 12. The foil for TEM observation was prepared from axial section of the crept specimen. It can be seen that the dislocations occupy the γ/γ' interfaces. As the foil cuts also part of the γ channel above the layer of γ' cubes seen in Fig. 12, the dislocations which seemingly lie within some of the γ' cubes are in fact dislocations lying in the γ channel above the observed layer of γ' cubes. Dislocation deposition at the γ/γ' interfaces was observed also in the regions of regular γ/γ' arrangement of the crept specimens of superalloy CM186LC. A different picture offer the regions where the γ' particles are very large. An example is shown in Fig. 13. A large γ' particle separated by γ channel can be seen. It is important, that the dislocations are present not only at the γ/γ' interfaces, but also in the interior of the γ' particle.

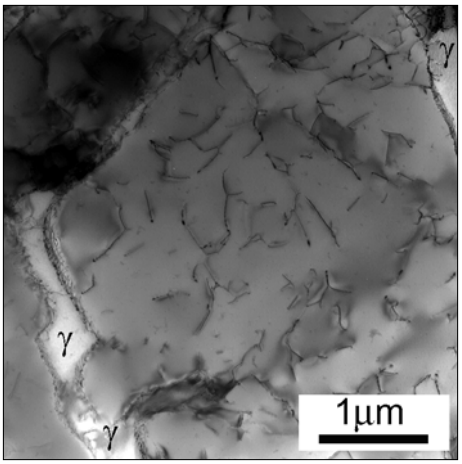

Fig. 13. Dislocation structure in eutectic region of a CM186LC specimen crept at 850 °C.

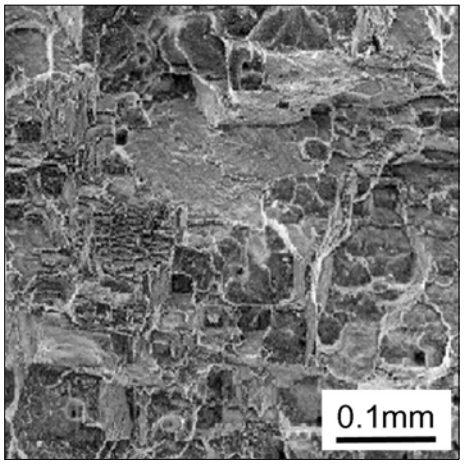

Fig. 14. SEM micrograph of fracture surface of a CMSX-4 specimen crept at 850 °C.

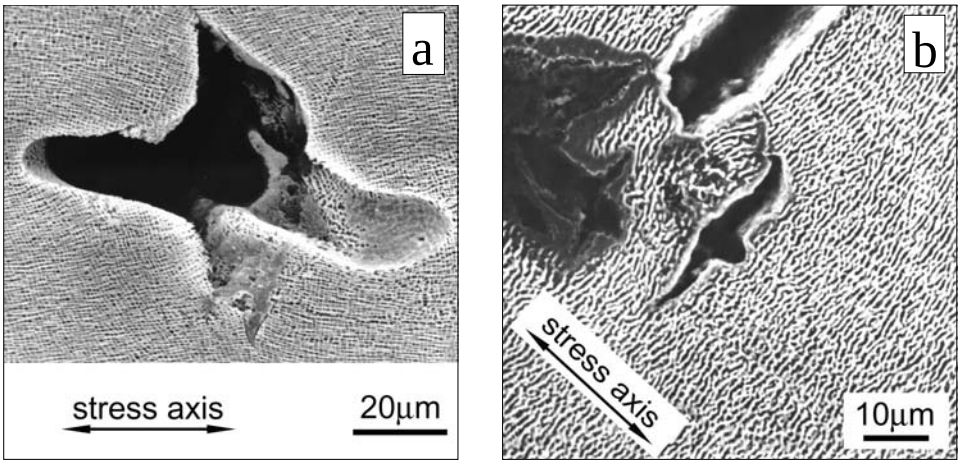

Fig. 15. Initiation of creep microcracks at casting pores in CMSX-4 specimens with the ⟨001⟩ orientation. (a) 850 °C, (b) 950 °C.

3.4 Fracture process

Fractography showed that the creep cracks initiate at casting pores, fractured carbides, and carbide/matrix interfaces, with propagation along (001) planes

(Fig. 14), perpendicular to the applied stress. The fracture surface morphology did not change substantially with test temperature and did not substantially differ for CMSX-4 and CM186LC. Some of the crept specimens were axially cut, ground and polished to observe details of the crack initiation. Figure 15 presents typical results for a temperature of 850 ℃ (no rafting, Fig. 15a) and 950 ℃ (expressive rafting, Fig. 15b). In both cases microcracks with sharp tips perpendicular to the stress axis are seen to initiate at casting pores (rounded peripheries). At 850 ℃ the γ/γ' morphology is cuboidal, at 950 ℃ a rafted γ/γ' morphology can be seen. The micrographs of the type shown in Fig. 15 suggest that the creep microcracks propagate along the γ channels.

3.5 Effect of notches on creep life

In this work the notch effect was determined at 850 ℃ for circumferential type of notch (for geometry of specimens see section 2). One example of results is shown in Fig. 16 for CM186LC with the axis orientation ⟨001⟩ in terms of dependence of time to rupture on net stress calculated as load divided by the initial cross-section area. It can be seen that for the same net stress the creep life of notched specimens is longer than that of smooth specimens. It means that the tested material exhibits under the given conditions a creep notch-strengthening behaviour. The same effect was observed for other orientations both for CM186LC and CMSX-4. This beneficial effect of circumferential notches on the creep life is due to the constraint of the plastic deformation in the triaxial stress field around the notch [10].

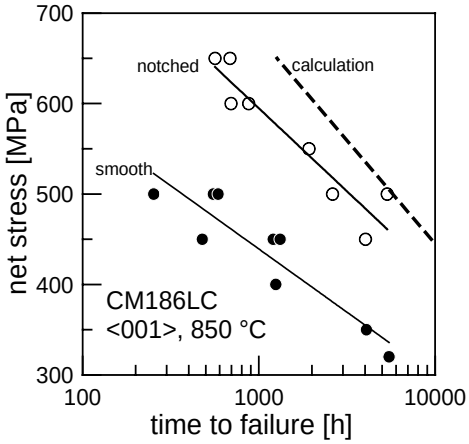

Fig. 16. Effect of notch on creep rupture curve.

In our previous work a method for the estimation of creep notch effect was proposed [10]. This method comes out from the standard creep data (determined on smooth specimens) and calculates the creep rupture curve of the notched specimens. The particular steps are as follows:

1. Determination of the stress and strain distribution in notched specimens by time-dependent elastic-plastic finite-element computation. As the input data, the experimentally determined stress dependence of the minimum creep rate for smooth specimens (see Fig. 7) is used.

2. As the computed stress and strain distribution reaches a steady state, it is possible to characterize the overall steady-state creep behaviour of the notched

specimen by the creep strain rate component in the direction of the applied stress. The average value of this strain rate component taken over the net-section plane is computed.

3. Using the Monkman-Grant's diagram determined for smooth specimens (see Fig. 8) the creep life corresponding to this average value is determined.

The result of such a calculation of the notched creep life is also shown in Fig. 16. It should be noted that the proposed evaluation represents an approximate assessment, not an exact determination. Similar or in some cases better approximations were found for other orientations.

4. Discussion

The results of creep tests for two single crystal superalloys clearly show that for the same crystal orientation, testing temperature and applied stress (i) the creep life of CMSX-4 is higher than that of CM186LC and (ii) the creep rate of CM186LC is higher than that of CMSX-4 for the whole lifetime. In other words, the creep resistance of CMSX-4 is superior to that of CM186LC. The reason is to be sought in the differences of the microstructure. While the CMSX-4 consists of regular distribution of γ' particles in γ matrix, the CM186LC consists not only of regions of regular γ/γ' distribution (75 to 80 % of the total volume), but also of eutectic regions with large and irregular γ' particles. TEM examination of virgin specimens found that the dislocation density is very low both in the regular and eutectic regions. As both the alloys are negative misfit alloys [3, 11], the effective stress at the outset of testing will be higher in the horizontal γ channels compared with the vertical γ channels. Thus, generation of dislocations starts in the horizontal channels and is followed by piling-up at the γ/γ' interfaces to reduce misfit strains. Dislocation creep is the dominant mechanism with dislocations moving by a combination of glide in the matrix, aided by climb and cross-slip processes along the γ/γ' interfaces to by-pass the particles and assist recovery processes, such as the reaction and annihilation of dislocations with opposite sign to decrease dislocation density. The size of the γ' particles in the eutectic colonies is sufficiently large for independent activation of dislocation sources within the γ' particles. Thus, deformation of the large γ' particles occurs independently of the deformation in the adjacent γ matrix and so contributes to the overall deformation of the specimen. This is the main reason for higher creep rate and consequently for shorter creep life in CM186LC as compared to CMSX-4. The slight differences in the chemical composition of the two alloys are believed not to play an important role.

To understand the effects of crystal orientation, temperature and applied stress on the creep behaviour it is necessary to take into account the whole spectrum of mechanisms involving

(a) dislocation slip in γ channels and deposition of dislocations on the γ/γ' interfaces,

(b) cutting of γ' particles by dislocations generated in γ channels,
(c) dynamic recovery of the dislocation structure,
(d) morphological changes of γ' particles by migration of γ/γ' interfaces,
(e) coarsening of the rafted structure.

Within the applied stress interval almost no dislocation cutting of the γ' particles was found for temperatures up to 850 ℃. This is in agreement with other observations [e.g. 12]. At 950 ℃ rafting for orientation $\langle 001 \rangle$ was observed (Figs. 9 and 10): the γ' particles form infinite thin plates (thickness ~ 0.5 μm) by means of stress and strain driven diffusion process. This closes many of the vertical γ channels and encourages cutting of the γ' rafts. The observation of dislocation structure by TEM shows that also in this case the dislocations are present mainly at the γ/γ' interfaces. The extremely large γ' particles in the eutectic colonies play a similar role as at lower temperatures, i.e. they contribute independently to the creep deformation.

The effect of orientation on creep deformation and fracture, in other words the pronounced creep anisotropy can be attributed to the orientation dependence of the superposition of the misfit and external stresses, leading to different dislocation configurations. At temperature of 950 ℃ also the orientation dependence of the rafting process also contributes to the overall creep anisotropy. There are microstructurally and phenomenologically based models of the creep anisotropy of the γ/γ' nickel-based superalloys, but none of them has been more broadly accepted.

The effect of notches on the creep rupture behaviour of uniaxially loaded bars has been experimentally studied on several materials including single-crystalline superalloys [10, 15]. The effect of notches on the creep rupture behaviour of uniaxially loaded bars made of creep-ductile materials can be both beneficial or detrimental in dependence on the material, notch geometry and testing conditions (temperature, applied load, surrounding environment). For the same net section stress (load divided by the minimum cross-section) the lifetime of the notched bar can be higher [e.g. 13] or lower than the lifetime of the smooth bar [e.g. 14]. The available data show that the most decisive factor for the notch behaviour is the degree of the stress triaxiality due to the presence of the notch. The axial plastic deformation is constrained in the triaxial stress-state field across the whole net section area. This is the reason why the lifetime in the case of circumferential notches leading to high-triaxiality (cylindrical bars) is higher than the lifetime in the case of through-the-thickness notches (plates) leading to low-triaxiality under the same net section stress and for a comparable stress concentration factor.

5. Conclusions

The results of creep tests and microstructural investigations obtained on two nickel base single crystal superalloys with different γ/γ' distribution can be summarized in the following way.

(a) For the same crystal orientation, testing temperature and applied stress it holds that (i) the creep life of CMSX-4 is higher than that of CM186LC and (ii) the creep rate of CM186LC is higher than that of CMSX-4 for the whole lifetime. It means that the creep resistance of CMSX-4 is superior to that of CM186LC.

(b) The reason is believed to lie in the deformation of the large γ' particles in CM186LC, which occurs independently of the deformation in the adjacent γ matrix and so contributes to the overall deformation of the specimen. In both the superalloys the major part of the creep deformation is due to dislocations originating and moving in the γ channels and occasionally cutting the γ' particles in the regions of regular γ/γ' distribution. The γ' particles in the eutectic colonies of CM186LC are sufficiently large for independent activation of dislocation sources within the γ' particles. This causes the additional deformation in CM186LC, which do not occur in CMSX-4.

(c) The ranking of orientations from the point of view of creep resistance is $\langle 111\rangle$, $\langle 001\rangle$, $\langle 011\rangle$. This holds for both the superalloys. The pronounced creep anisotropy can be attributed to the orientation dependence of the superposition of the misfit and external stresses, leading to different dislocation configurations.

(d) The effect of circumferential notches on the creep rupture behaviour of uniaxially loaded cylindrical bars is beneficial. The method for the assessment of the notched creep behaviour on the basis of the standard smooth specimen creep data can serve as useful approximate estimation.

(e) The creep cracks initiate at casting pores, fractured carbides, and carbide/matrix interfaces. The fracture surface morphology does not change substantially with test temperature and does not substantially differ for CMSX-4 and CM186LC alloys.

Acknowledgements

This research was supported by the Academy of Sciences of the Czech Republic under the contracts AV0Z20410507 and 1QS200410502. This support is gratefully acknowledged.

REFERENCES

[1] GOLDSCHMIDT, D.: In: Materials for Advanced Power Engineering. Eds.: Coutsouradis, D. et al. Dordrecht, Kluwer Academic Publishers 1994, p. 661.

[2] SCHNEIDER, W.—MUGHRABI, H.: In: Creep and Fracture of Engineering Materials and Structures. Eds.: Wilshire, B., Evans, R. W. London, The Institute of Materials 1993, p. 209.

[3] WILCOCK, I. M.—LUKÁŠ, P.—MALDINI, M.—KLABBERS, J.—DUBIEL, B.—HENDERSON, M. B.: In: Materials for Advanced Power Engineering 2002. Eds.: Lecomte-Beckers, J. et al. Forschungszentrum Jülich 2002, Part 1, p. 139.

[4] LUKÁŠ, P.—KUNZ, L.—SVOBODA, M.—ČADEK, J.: Mater. Sci. Forum, *482*, 2005, p. 267.

[5] DUBIEL, B.—CZYRSKA-FILEMONOWICZ, A.: Mater. Chem. Phys., *81*, 2003, p. 427.

[6] BULLOUGH, C. K.—TOULIOS, M.—OEHL, M.—LUKÁŠ, P.: In: Materials for Advanced Power Engineering 1998. Eds.: Lecomte-Beckers, J., Schubert, F., Ennis, P. J. Forschungszentrum Jülich 1998, Part 2, p. 861.
[7] PILKEY, W. D.: Peterson's Stress Concentration Factors. New York, Wiley Interscience Publication 1997.
[8] MUGHRABI, H.—TETZLAFF, U.: Advanced Eng. Mater., *6*, 2000, p. 319.
[9] MALDINI, M.—LUPINC, V.—ANGELLA, G.: Kovove Mater., *42*, 2004, p. 21.
[10] LUKÁŠ, P.—PRECLÍK, P.—ČADEK, J.: Mater. Sci. Eng., *A298*, 2001, p. 84.
[11] VÖLKL, R.—GLATZEL, U.—FELLER-KNIEPMEIER, M.: Acta Mater., *46*, 1998, p. 4395.
[12] POLLOCK, T. M.—ARGON, A. S.: Acta Metall. Mater., *40*, 1992, p. 1.
[13] EGGELER, G.—TATO, W.—JEMMELY, P.—DEMESTRAL, B.: Scripta Metal. Mater., *27*, 1992, p. 1091.
[14] KONISH, H. J.: J. Pressure Vessel Technology, *110*, 1988, p. 314.
[15] ARDAKANI, M. G.—BASOALTO, H.—SHOLLOCK, B. A.—McLEAN, M.: Mater. Sci. Forum, *426–432*, 2003, p. 797.